ORGANIC CHEMISTRY FRONTIERS

CHINESE CHEMICAL SOCIETY

ROYAL SOCIETY OF CHEMISTRY

Topomeric Aza/Thia Cryptands: Synthesis and Theoretical Aspects of In/Out Isomerism using n-Alkyl Bridging

Journal:	*Organic Chemistry Frontiers*
Manuscript ID	QO-RES-01-2020-000123.R1
Article Type:	Research Article
Date Submitted by the Author:	12-Mar-2020
Complete List of Authors:	Taschner, Ian; Indiana University Northwest, Chemistry Walker, Tia; Indiana University Northwest, Chemistry Mallojjala, Sharath Chandra; University of Georgia, Department of Chemistry; Texas A&M University, Department of Chemistry Schrage, Briana; University of Akron, Chemistry Ziegler, Christopher; University of Akron, Department of Chemistry Gao, Xinfeng; Indiana University, Chemistry Wheeler, Steven; University of Georgia, Center for Computational Quantum Chemistry

Title: Topomeric Aza/Thia Cryptands: Synthesis and Theoretical Aspects of *In/Out* Isomerism using n-Alkyl Bridging

Authors:
Ian S. Taschner[a*], Tia L. Walker[a], M. Sharath Chandra[d], Briana R. Schrage[b], Christopher J. Ziegler[b], Xinfeng Gao[c], and Steven E. Wheeler[d]

[a] Department of Chemistry, Indiana University Northwest, Gary, Indiana 46408
[b] Department of Chemistry, The University of Akron, Akron, Ohio 44325
[c] Department of Chemistry, Indiana University Bloomington, Bloomington, Indiana 47405
[d] Center for Computational Quantum Chemistry, Department of Chemistry, University of Georgia, Athens, Georgia 30602

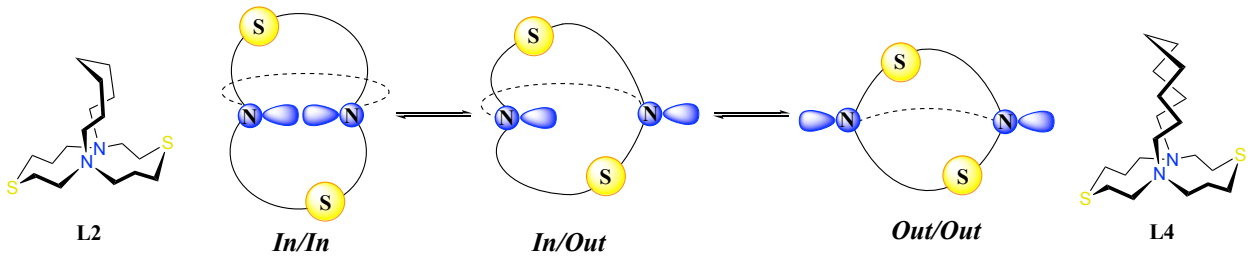

Abstract:
A series of heterobicyclic aza/thia-lactams and cryptands incorporating changes in n-alkyl bridging length have been synthesized, characterized, chelated to heavy metals and computationally assessed. Spectroscopic analysis of aza/thia-lactams **L1** and **L3** revealed multiple conformational isomers, due to rotameric perturbations associated with the amide bond. Correlation spectroscopy on amine cryptands **L2** and **L4** supported the presence of intrinsic topological chirality, resulting from a preferred orientation of the amine lone pairs in solution. The unique magnetic environments observed in ^{1}H NMR were attributed to the electron density inside the crypt, which adopt a nephroidal-epicycloid structure with two nitrogen atoms representing the cusps. The major conformational and constitutional isomers for **L2** and **L4** present in solution were determined to be the *in/in* pair of enantiomers (R,R and S,S) and confirmed through computational analysis. Application of ligands **L1-L4** as heavy metal chelates was addressed using Pb(II), Hg(II), Cd(II) and Ag(I) through NMR spectroscopy and mass spectroscopy.

Introduction:
The field of supramolecular chemistry has been expanding and evolving since the initial crown ethers and cryptands first synthesized by Pedersen,[1] Lehn,[2] and Cram.[3] Cryptands with nitrogen atoms occupying the pivot point have provided scaffolds for stabilization of metals in unique oxidation states[4] and encapsulation of select ions which increases solubility in aqueous media.[5] Host-guest chemistry associated with cryptands continues to be a progressive and important field. Cryptands have been recognized for their ability to act as a three-dimensional scaffolds for host-guest chemistry,[6] metal chelation,[7] biomedical imaging,[8] and self-assembly.[9] The development of new macro-heterobicyclic compounds are critical for oncological studies,[10] sensors,[11] and bivalent chelators.[12]

Dithiosemicarbazones, such as diacetyl-bis(N4-methyl-3-thiosemicarbazone have been complexed with ^{64}Cu (ATSM ^{64}Cu(II)) which are currently under investigation as radiotracers for tissue hypoxia (Fig. 1).[13] Increased selectivity and cell permeability results from ligand modification which imparts stability towards cellular redox processes.[13,14] By comparison, Weisman and Wong have focused their efforts on the construction of bicyclic polyamines.[15] The use of their 14-membered cross-bridged cyclam ligand has shown great promise as a chelate of radiolabeled copper for PET imaging.[16] The design of the three-dimensional tetra-aza macrocycle has played a major role in copper radiopharmaceuticals and this compound can be tethered to a directing peptide for delivery into target tissues and organs.[17] Cryptand molecules may be suitable ligands for ^{64}Cu chelation, as they have historically shown strong binding of Cu(II) cations and impart kinetic inertness.[18] Having access to the 14-membered N_2S_2 scaffold 1,8-dithia-4,11-diazacyclotetradecane (Fig. 1), attempts to elucidate the kinetic stability through tuning on the lone pair positions was undertaken.

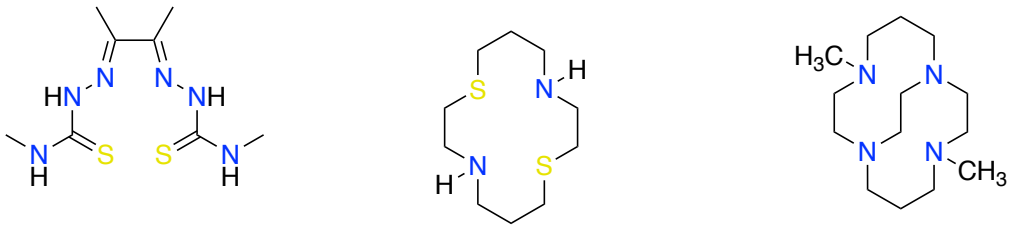

bis(thiosemicarbazonate) ATSMH$_2$ | N_2S_2 1 | (4,11-dimethyl) cross-bridged cyclam N_4

Figure 1. Structure of diacetyl-bis(N4-methyl-3-thiosemicarbaone) (ATSMH$_2$), 1,8-diathia-4,11-diazacyclotetradecane (N_2S_2), and 4,11-dimethyl-1,4,8,11-tetraazabicyclo[6.6.2]hexadecane ((4,11-dimethyl) cross-bridged cyclam N_4)

The chemical topology of Weissman and Wong's cross bridged tetra-aza macrocycle was engineered to constrain the directionality of chelation to afford stable metal ligates. Examination of cryptand crystal structures reported in literature indicate a preference for nitrogen lone pair orientation to reside within the scaffold of medium sized bicycles, geometrically representing a nephroidal motif (Fig. 2).[19] To better understand tunability with respect to the lone-pair orientation, the bridge head was modified by varying the carbon chains of the NS system.

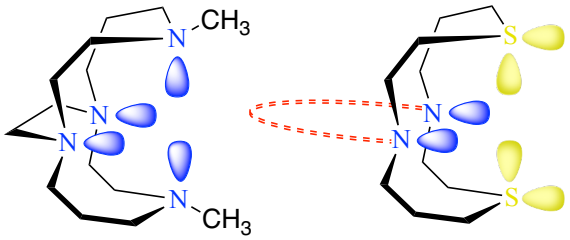

Cross-bridged cyclam | N_2S_2 Cryptand

Figure 2. Proposed lone pair orientation of N_2S_2 upon bridging of the nitrogen atoms with respect to cross bridged cyclam

Cryptands containing bridgehead nitrogen atoms have been reported to have a bias in respect to the lone pair orientation (*in/in, in/out,* and *out/out*) and has been computationally addressed by Auffinger *et al*[20]. and reviewed extensively by Alder *et al*[21] . Of the three possible topomers, *in/in*

has been shown to be the predominate conformation in solution and solid state (Fig. 3) for medium sized rings.[22] The conformational bias for the *in/in* topomer observed through NMR analysis was mechanistically determined to undergo topomerization through lone-pair inversion, adopting a low-lying confirmation where the bridgehead lone pairs are identical through symmetry. Through heteronuclear correlation spectroscopy, the reported aza/thia cryptands were determined to predominately exist as one topomer at 25 °C, which imparts a chiral environment in which geminal methylene protons are diastereotopic and conformationally restricted. Rotational interconversion of select methylene protons may also be constrained by the lone pairs on sulfur or a conformational bias between sulfur and/or nitrogen.[23] Due to the scarcity of sulfur containing aza-cryptands in literature, investigation of physical and chemical properties will aid in providing structures with discrete metal affinity and stability. Comprehensive *ab initio* density functional theory (DFT) incorporating solvent media effects was applied to these compounds to elucidate ring strain and pore size. Using NMR spectroscopy four diamagnetic metals (lead, mercury, silver, and cadmium) were chelated. Herein, we report the synthesis and computational characterization of **L1-L4,** X-ray structures of the macrocyclic lactams **L1** and **L3** as well as cryptand **L2** were obtained along with full NMR elucidation of amine cryptands **L2** and **L4**.

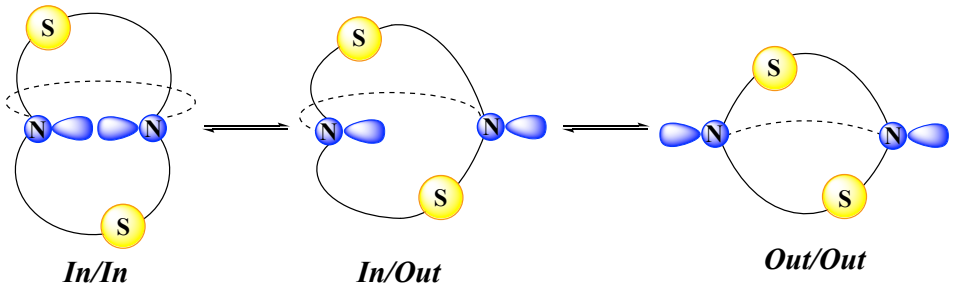

Figure 3. Nitrogen inversion of nephroidal topomers

Results and Discussion

Cryptands have provided many synthetic and spectroscopic challenges ranging from poor yields to unresolved frequencies in NMR spectroscopy.[24] Synthesis of the core aza-thia macrocycle, dithiacyclam (**1**), was completed in eight steps following the procedure outlined by Walker et al.[25] Condensation of bis-acid chlorides derived from pimelic and azelaic acids furnished bicyclic lactams **L1** and **L3**. Following Dietrich's strategic method for macrocyclization, high dilution in tandem with simultaneous addition of electrophile and nucleophile,[26] heterobicycles **L1** and **L3** were isolated in appreciable yields coinciding with literature values (Scheme 1).

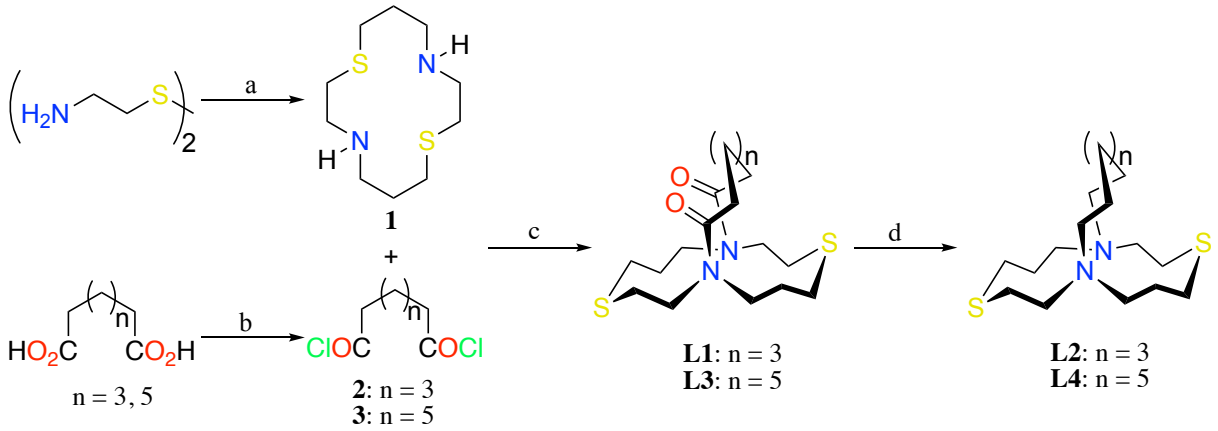

Scheme 1. Synthesis of Aza-Thia Cryptands L1 – L4. a. Reference 19; b. CH_2Cl_2, $SOCl_2$, 40 °C; c. **2** (n = 3) or **3** (n = 5), NEt_3, PhMe, 23°C, 48 h; d. BH_3·DMS, PhMe, 110 °C, 1 h; PhMe, Triethanol amine, 110 °C, 6 h.

Pimelic and azelaic acid were individually exposed to thionyl chloride in methylene chloride to afford *bis*-acid chlorides **2** and **3**, respectively (Scheme 1). The derived *bis*-acid chlorides were then independently subjected to a macrocyclization without further purification. Optimization of reaction conditions was crucial in order to obtain cryptands **L1** and **L3** in adequate yields. Precision syringe pumps were implemented to control the rate of addition of both dithiacylam **1** and *bis*-acid chloride (**2** or **3**). This set-up provided optimal yields for **L1** and **L3**, 29% and 48% respectively. The direct addition of silica gel to the reaction flask followed by concentration and column chromatography removed the need for aqueous work-up.

Yields were lower when utilizing pimeloyl chloride, possibly due to steric/entropic constraints during the intramolecular acylation. Evidence for incomplete cyclization can be rationalized using crystal structure data for hetero macrocycle **1** as a visual template. Lone pairs associated with the nitrogen atoms of **1** are antipodal with respect to one another and require inversion to afford the secondary macrocyclization (Fig. 4).[25] The proper alignment required to favor intramolecular cyclization could hinder the shorter carbon chains and favor intermolecular oligomerization.

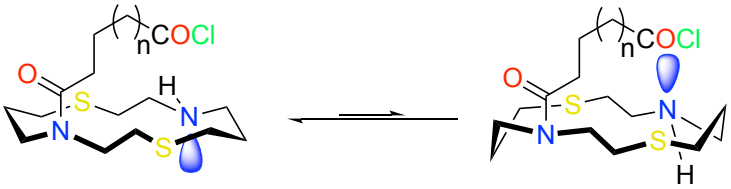

Figure 4. Lone pair alignment

Running the reaction for 48 h at 23 °C with a final concentration of 0.01 M (with respect to **1**) provided an increase in yield in both **L1** (38%) and **L3** (62%). To help elucidate the entropic barrier for cyclization under the optimized reaction conditions, glutaroyl chloride was introduced as the electrophile. The reaction did not provide any cryptand formation as solely oligomeric byproducts were observed. Bicyclic bis-lactams **L1** and **L3** were subjected to a borane reduction to afford the corresponding cryptands in 82% and 68%, respectively.

Full assignment of proton and carbon nuclei for cryptands **L2** and **L4** was assessed *via* homo/hetero nuclear correlation spectroscopy. The observed ^{1}H resonances of cryptands can be difficult to predict and compute based on conformational mobility restriction hindering rotational averaging of chemical shift effects. The lone pairs on nitrogen and sulfur contribute to additional chemical shift effects depending on topological alignment with corresponding protons. The ^{1}H NMR spectra for the 9-carbon bridge lactam **L3** could not be resolved, even at 115 °C in DMSO-d_6. The 7-carbon bridge lactam **L1** gave rise to multiple frequencies in the ^{1}H NMR that were attributed to multiple rotamers present in solution at 25°C. The ^{13}C NMR spectra of **L1** provided a distinct set of frequencies associated with a major topomer possibly due to the rigidity of the system. Analysis of cryptands **L2** and **L4** was challenging in deuterated chloroform due to overlapping ^{1}H-^{13}C correlation signals. To address this issue, NMR spectra of dichloride salts **L2-HCl** and **L4-HCl** in D_2O allowed for full identification of each signal in the ^{1}H and ^{13}C NMR spectra.

Cryptand **L4-HCl** NMR spectra elucidation was done at 25 °C using ^{1}H, ^{13}C, gCOSY, gHSQC, and gHMBC (Fig. 5). To help with analysis, a quantitative ^{13}C NMR experiment was performed and due to the symmetrical nature of **L4-HCl**, carbon #1 could easily be identified. Using carbon #1 as an initial bench mark, the remaining proton and carbon resonances could be assigned.

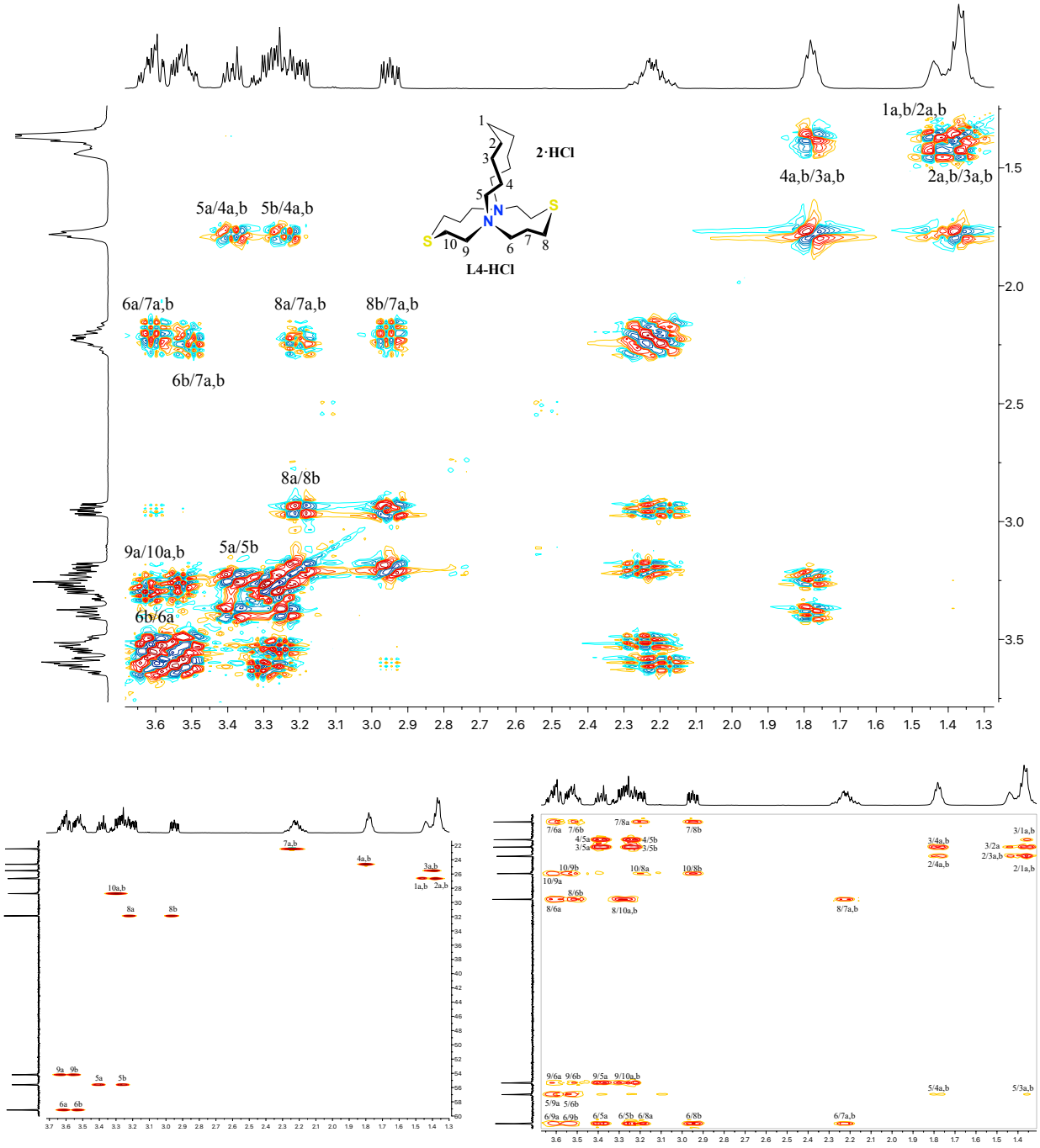

Figure 5. Top image depicts 2D-COSY NMR spectra of L4-HCl. Bottom Left, 2D-HSQC and Bottom Right 2D-HMBC. All samples were obtained in D_2O at 25°C.

The unique magnetic environments present in **L4-HCl** are apparent through gHSQC correlation spectroscopy and provide explicit evidence for a major topological isomer. Each unique ^{13}C nuclei is correlated to a pair of ^{1}H nuclei at differing frequencies. The Δν between ^{1}H methylene units increase with increasing bond distance from heteroatoms. The freebase **L4** also displayed this trend, which suggests a preference for *in/in* topology, in accordance with the literature.[27] *In/Out* isomerism at 25 °C on the NMR time scale (> 10^6) depicted one major topomer intrinsic to **L2** and **L4**. This data further supports *in/in* topology containing a C2 axis of rotation and observed topicity induced from localization of the lone pairs on the nitrogen nuclei.

The 7-carbon bridged **L2-HCl** was not fully soluble in D_2O at 25 °C and depicted multiple chemical conformations in solution. When the solution was heated to 45 °C, **L2-HCl** dissolved completely and remained in solution even when cooled back to 25 °C. The NMR experiments were then performed a second time to observe the solvated **L2-HCl** (Fig. 6). Using carbon #1 as the starting frequency, all protons and carbon nuclei were assigned (Table 1). The largest Δν between geminal diastereotopic protons of the 9-carbon bridged **L4-HCl** was observed on the carbon atoms directly attached to a heteroatom, presumably due to restricted rotation forcing one proton inside the crypt. Due to the stability of the *in/in* topomer associated with **L4-HCl**, ν_{obs} for geminal protons 8a and 8b were the greatest with a frequency difference of 124 Hz. Cryptand **L2-HCl** had the greatest Δν values between geminal diastereotopic protons with the largest frequency difference of 168 Hz. Interestingly, protons 3a and 3b (**L2-HCl**) exhibited a large Δν which could arise from an adopted nephroidal topology. These protons may be rigidly held in position from entropically favorable transannular interactions that are strongly driven by strain relief.

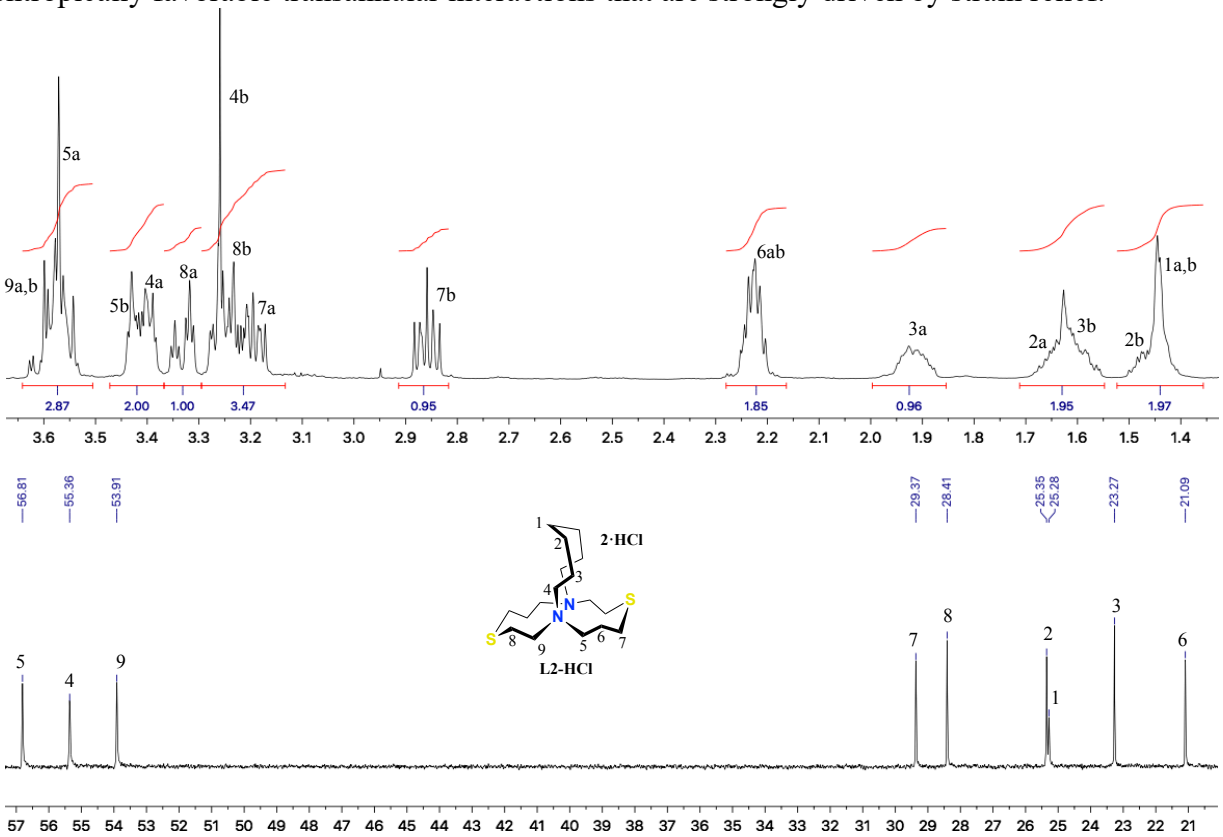

Figure 6. ^{1}H and ^{13}C frequencies of L2-HCl at 25°C in D_2O

Table 1. ^{1}H, ^{13}C frequencies and Δν (Hz) at 500 MHz for compounds L2-HCl and L4-HCl

1H a, b	1	2	3	4	5	6	7	8	9	10
ppm (a, b)										
L4-HCl	1.44, 1.43	1.36, 1.35	1.39, 1.37	1.79, 1.77	3.39, 3.23	3.60, 3.51	2.25, 2.19	3.20, 2.95	3.62, 3.54	3.33, 3.28
L2-HCl	1.44, 1.45	1.65, 1.48	1.93, 1.59	3.40, 3.25	3.57, 3.42	2.24, 2.21	3.20, 2.86	3.33, 3.22	3.61, 3.59	
Δν (Hz) of a, b										
L4-HCl	3	3	7	12	80	41	29	124	41	25
L2	2	89	166	75	74	15	168	50	7	

Crystals of **L1** and **L3** suitable for X-ray diffraction were grown from an ethyl acetate/pentane diffusion chamber at 23 °C and the elucidated structures were further probed computationally. Crystals of cryptand **L2** were obtained from DMSO-*d6* at 23 °C over a 72 h period. The crystal structures are depicted in Fig. 7 with relevant crystal and data collection parameters found in Table 2. Perturbation of the N_2S_2 core was observed in heterobicycle **L1** and **L2**, where the two sulfur atoms are on the same face of the bicycle (Fig. 7). Of the two amide ligands, **L1** shows some similarity with respect to the orientation of the sulfur atoms compared to the cross-bridged cyclam. The nitrogen atoms in **L1** was found by X-ray structure determination to have nearly planar nitrogen atoms, where the C-N-C angles average ~119° with the lone pair electrons orientated *in/in* with respect to one another (Table 3). With the addition of two extra carbon atoms in the bridgehead, the N···N distance decreased by ~0.4 Å from ~5.3 Å to ~4.9 Å and the S···S significantly increased by ~0.9 Å. This differs from the cross bridged cyclam where the pore measures ~ 2.9 Å for the bridgehead nitrogen atoms and ~4.0 Å for the methylated amines. The cyclam has less planarity than **L1** and **L3** where the C-N-C angles range from 110°-112° similar to **L2**. Crystal structures of ATSM-Cu(II) are more comparable to the cross-bridged cyclam with N···N distances ~2.5 Å and N···S distances ~4.2 Å. Unlike the cyclam however, ATSM-Cu(II) C-N-Cu and N-N-Cu has greater planarity (~120°) likely due to the square planar coordination of copper.[13]

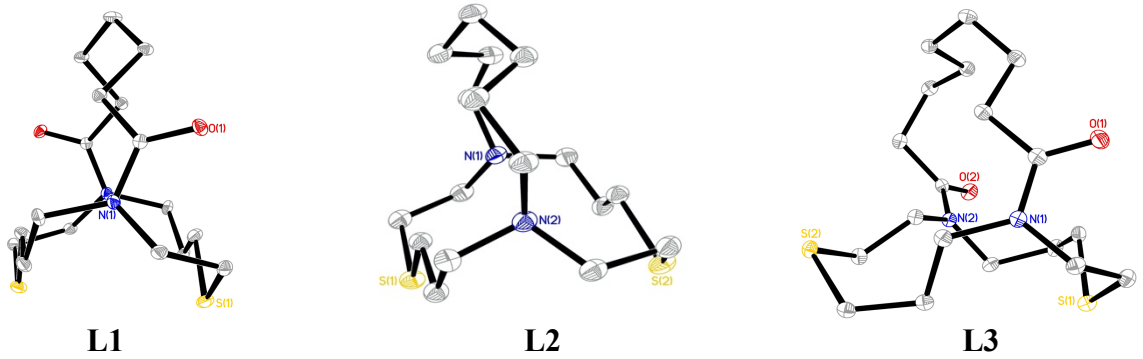

Figure 7. The thermal ellipsoid diagram of 7-carbon bridge amide (L1), 7-carbon bridge amine (L2) and 9-carbon bridge amide (L3) with 35% probability displacement ellipsoids. For clarity the hydrogen atoms on the carbon positions have been omitted. CCDC: 1979275 (L1), 1989498 (L2) and 1979276 (L3)

To determine if substituting carbon for sulfur in the bridgehead effects the overall structure, cryptand **L3** was compared to previously reported sulfur bridging system (**L5**).[28] Interestingly, **L3**

showed minimal structural changes to the bridge, and no changes to the N_2S_2 parent scaffold (Fig. 8). The presence of bridging sulfur atoms electron densities changes the directionality of the 3-carbon atoms but leaves the overall molecular configuration intact. **L3** was identical to **L5** when comparing the S···S, and N···N distances, with only minimal changes in the C-N-C angles (Table 3). With exchange of the two sulfur atoms for carbons, no spatial changes occurred to the N-C-C-S with preservation of one anti and one gauche orientation. Due to minimal structural changes with conservation of orientation it could be implied that the sulfur atoms in **L5** do not impart much structural control. We would however expect differences in metal chelation to occur as **L3** does not contain the additional propensity imparted by the sulfur atoms to bind to heavy metals.

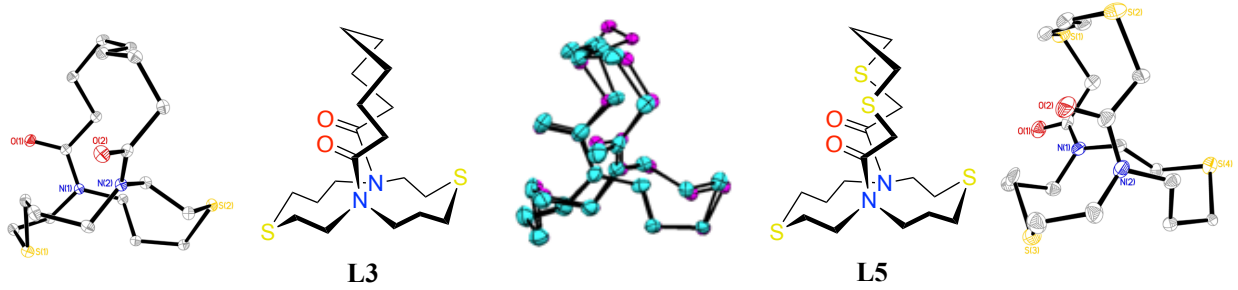

Figure 8. Thermal ellipsoid drawing for **L5** at 35% probability with hydrogen atoms omitted for clarity. Structural overlay of L1 (Pink) with L5 (Blue) showing structural preservation of the N_2S_2 pore is shown in center using CCD 1576451.[28]

Table 2. X-ray data collection and structure parameters for amide bridging C7 (L1) and C9 (L3) and amine C7 (L2)

Complex	**L1**	**L2**	**L3**
Empirical formula	$C_{17}H_{30}N_2O_2S_2$	$C_{17}H_{34}N_2S_2$	$C_{19}H_{34}N_2O_2S_2$
Formula weight	358.55	330.58	386.60
Crystal System	Monoclinic	Triclinic	Monoclinic
Space group	C2/c	P-1	$P2_1/n$
a/Å	12.2727(5)	9.8079(14)	15.65(4)
b/Å	9.4046(4)	10.0730(14)	8.31(2)
c/Å	15.4138(6)	10.1224(15)	16.92(4)
a/°	90	106.418(5)	90
β/°	92.276(2)	103.585(6)	113.56(3)
γ/°	90	90.063(6)	90
Volume (Å^3)	1777.65(13)	930.0(2)	2017(9)
Z	4	2	4
D_{calcd}/mg m^{-3}	1.340	1.181	1.273
μ(Mo Kα)/mm^{-1}	0.311	0.284	0.279
F(000)	776	364	840
reflns collected	16118	26342	22620
indep. reflns	2244	4627	2960
GOF on F^2	1.029	1.113	1.073
R1 (on F_o^2, I > 2σ(I))	0.0296	0.0472	0.0292
wR2 (on F_o^2, I > 2σ(I))	0.0738	0.1135	0.0716
R1 (all data)	0.0354	0.0730	0.0333
wR2 (all data)	0.0772	0.1203	0.0764

Complex	**L1**	**L2**	**L3**
Empirical formula	$C_{17}H_{30}N_2O_2S_2$	$C_{17}H_{34}N_2S_2$	$C_{19}H_{34}N_2O_2S_2$
Formula weight	358.55	330.58	386.60
Crystal System	Monoclinic	Triclinic	Monoclinic
Space group	C2/c	P-1	$P2_1/n$
a/Å	12.2727(5)	9.8079(14)	15.65(4)
b/Å	9.4046(4)	10.0730(14)	8.31(2)
c/Å	15.4138(6)	10.1224(15)	16.92(4)
a/°	90	106.418(5)	90
β/°	92.276(2)	103.585(6)	113.56(3)
γ/°	90	90.063(6)	90
Volume (Å^3)	1777.65(13)	930.0(2)	2017(9)
Z	4	2	4
D_{calcd}/mg m^{-3}	1.340	1.181	1.273
μ(Mo Kα)/mm^{-1}	0.311	0.284	0.279
F(000)	776	364	840
reflns collected	16118	26342	22620
indep. reflns	2244	4627	2960
GOF on F^2	1.029	1.113	1.073
R1 (on F_o^2, I > 2σ(I))	0.0296	0.0472	0.0292
wR2 (on F_o^2, I > 2σ(I))	0.0738	0.1135	0.0716
R1 (all data)	0.0354	0.0730	0.0333
wR2 (all data)	0.0772	0.1203	0.0764

Computed solution phase geometries (in chloroform) for **L1**, **L2**, **L3**, **L4** are shown below (Fig. 9). Moreover, two new cryptands **L6** and **L7** were also probed computationally to develop a broader understanding for pore size dependence and rotamer interconversion due to the changes in the bridging system. The computed geometries of **L1, L2** and **L3** were in good agreement with reported X-ray crystallographic structures. It was observed that the major rotamer for the smaller bicyclic lactams preferred the carbonyl groups pointing in the opposite direction in contrast to **L3** and **L5**. This might be due to the smaller pore size in lactams **L1** and **L6** in comparison to **L3** and **L5** (Table 3), thereby forcing the carbonyl units to adopt an antipodal alignment with respect to

one another. The structural alignment and electronics indicated a diametric relationship between the amide carbonyl's dipole. When **L1**'s amide carbonyl dipoles are parallel, as shown in Fig. 10 (**LR1**) the sulfur atoms lie on opposite planes with respect to the N_2S_2 core. Major rotamers of **L3** in the solution phase were identified using density functional theory (DFT; see the computational details below).

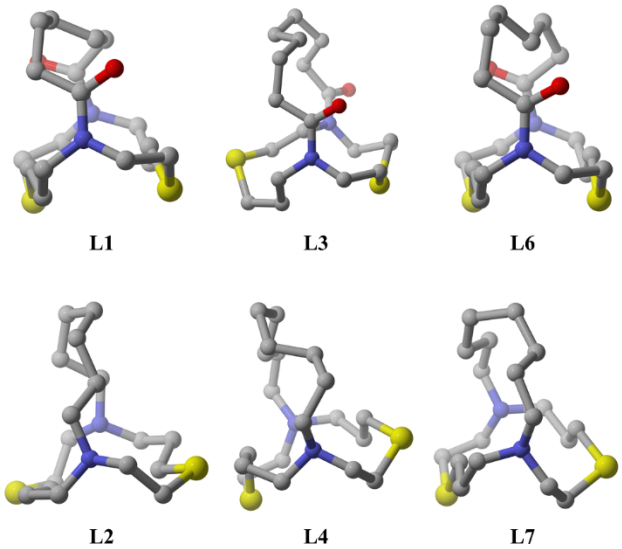

Figure 9. Solution phase geometries computed at PCM: Chloroform ωB97X-D/def2-TZVP/B97-D/def2-TZVP of cryptands L1 through L7

Furthermore, the bicyclic thia-lactams (**L1**, **L3**, and **L6**) are predicted to exist in two rotameric conformations (**Lx** and **LRx**; x = 1, 3, and 6). These rotamers are primarily differentiated based on the relative orientation of the carbonyl group, and the computed electronic energy barriers for the interconversion between these rotamers were found to decrease with decreasing bridge length (Fig. 10).

Table 3. Distances and sum of the C-N-C angles (°) in the computed solution phase geometries.

Compound	L1*	L1	L2*	L2	L3*	L3	L4	L5[28]	L5[28]	L6	L7
N···N [Å]	5.31	5.50	5.05	4.59	4.9	4.96	5.20	4.8	4.68	5.78	5.03
S···S [Å]	4.90	4.71	6.06	6.40	5.8	5.57	5.67	5.8	6.01	4.44	5.58
(ΣωN)	357	357, 357	331, 332	341, 333	358, 360	360, 357	331, 332	354, 359	357, 360	358, 357	334, 332

*Calculated from X-ray crystal structures for comparison

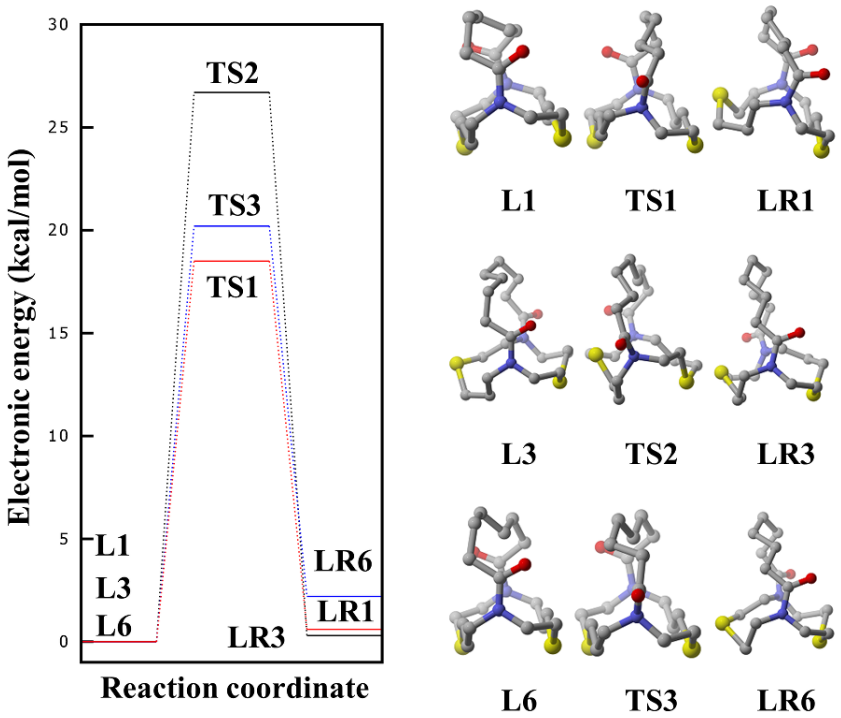

Figure 10. Solution phase rotameric barriers for the bicyclic thia-lactams reported in this study.

Sulfur-donor macrocycles have shown to form unique topological complexes with soft d-block metals,[29] resulting in unique supramolecular complexes. The metal ion is forced to adopt an exocyclic coordination resulting in discrete metallo suprastructures with atypical stoichiometries.[30] Macrocyclic ligands **L1-L4** were subjected to heavy metal chelation with Pb(II), Hg(II), Cd(II) and Ag(I) in a 1:1 stoichiometric ratio. Binding was analyzed through NMR spectroscopy and mass spectroscopy.

The induced shift of nuclear frequencies observed within the ^{1}H NMR spectra of **L1** and **L3** with silver(I) triflate and mercury(II) nitrate provided evidence for complexation. High resolution mass spectroscopy further identified two different stoichiometric lactam:metal chelates, 1:1 and 2:1 for silver and mercury. When Pb(II) nitrate and cadmium chloride were introduced to **L1** and **L3** under the same conditions at the same concentration, no change in chemical shifts were observed. High resolution mass spectroscopy indicated minimal complexation of **L1** and **L3** with Pb(II) and predominately produced free metal and lactam. Cadmium(II) chloride did not show signs of complexation in ^{1}H NMR or mass spectroscopy. Interestingly, ^{13}C NMR of **L1** and **L3** in the presence of Cd(II) had a dramatic increase in signal to noise compared to the lactams with no Cd(II) present at the same concentration in DMSO-*d6*.

Complexation studies of cryptands **L2** and **L4** (Figure 11) exhibited similar nuclear frequency shifts as their lactam counterparts. Silver and mercury both indicated complexation with **L2** and **L4** in both ^{1}H and ^{13}C NMR. The ^{13}C NMR of both ligands in the presence of silver indicated multiple conformations splitting the ^{13}C signals into multiple sets and due to metal-ligand exchange certain frequencies were broadened. Lead and cadmium both did not provide any

perturbations in ^{1}H spectra and the ^{13}C spectra had a similar increase in resolution as the macrocyclic lactams described above.

Attempts to obtain crystal structures of **L1-L4** with Pb(II), Hg(II), Cd(II) and Ag(I) were unsuccessful. To better understand ligand:metal binding, ion capture applications using **L4** were explored by a preliminary computational study of gas phase binding energies with copper(I) and silver(I) ions. Gas phase binding energies were computed for both monomeric M(**L4**) and dimeric M(**L4**)$_2$ complexes (Figure 11). The computed binding data was not statistically different between monomeric and dimeric complexes, supporting HRMS data obtained for silver(I). This data further suggests that copper(I) will bind more strongly to **L4** than silver, warranting further investigation into copper chelation. Comparing the computed binding data of **L4** to the literature gas phase binding energies of 4,7,13,16,21,24-hexaoxa-1,10-diazabicyclo [8,8,8] hexacosan ([2.2.2]) with alkali metal ions,[31] **L4** was identified to bind more strongly. From this, we can conclude that these new heterobicyclic systems show promising metal binding affinities. Further studies involving heavy metals and other ions of interest are underway.

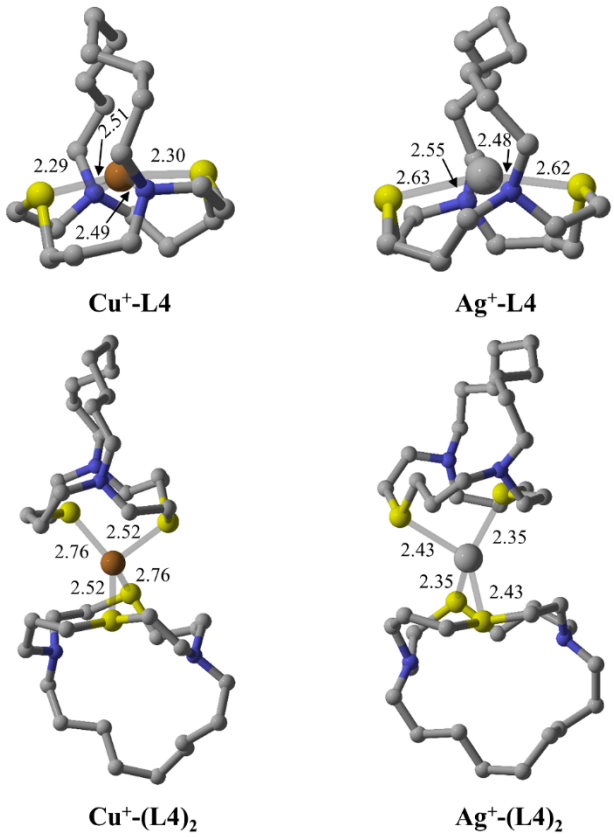

Figure 11. Computed metal binding for both copper(I) and silver(I) with **L4** showing both monomeric and dimeric forms.

Table 4. Computed gas phase binding energies of **L4** with silver(I) and copper(I) compared with 4,7,13,16,21,24-hexaoxa-1,10-diazabicyclo [8,8,8] hexacosan ([2.2.2]).

Complex	Binding Energy (kcal/mol)
K^+ [2.2.2]	-83.1
Na^+[2.2.2]	-69.7
Cu^+(**L4**)	-141.2
Cu^+(**L4**)$_2$	-127.7
Ag^+(**L4**)	-112.8
Ag^+(**L4**)$_2$	-100.9

In conclusion, two bicyclic thia-lactams (**L1** and **L3**) and two aza/thia cryptands (**L2** and **L4**) have successfully been synthesized and all protons and carbon atom positions were observed using heteronuclear NMR correlation spectroscopy. The gross impact of computational chemistry on conformational perturbations has been improving with larger data sets available. Through DFT calculations, the structures of **L1** and **L3** were modeled and matched with the observed conformations from X-ray data. Computational assessment provided localized structural conformations depicting major changes in the amide carbonyl's respective orientation on carbon bridges ranging from 7-9 carbon atoms. Using both computation and X-ray structure elucidation, the 7-carbon amide containing bridge may be better suited to chelate copper due to the resultant heteroatom orientation. Decreasing the number of atoms in the carbon bridge would reduce pore size, potentially giving rise to structures more consistent with that of the cyclam cross-bridge. Host-guest applications with specific cations[32] or anions[33] may alter the electronics, allowing for enthalpically mediated guest specificity. Metal selectivity integrated into cryptands can be enhanced or suppressed based on pore size and heteroatom placement, further improving ligand engineering. Chelation experiments using d-block metals such as copper and nickel for ligands **L1-L4** will be further investigated.

Experimental

12,18-dithia-1,9-diazabicyclo[7.6.6]henicosane-2,8-dione (L1). A 300 mL flame-dried 3-neck round-bottom flask equipped with a magnetic stir bar, nitrogen inlet, and three septa was charged with dry toluene (75 mL). A gas-tight syringe charged with 1,8-dithia-4,11-diazacyclotetradecane (0.352 g, 0.0015 mol), triethylamine (0.44 mL, 0.0030 mol) in toluene (37.5 mL) and a second gas-tight syringe was charged with pimeloyl chloride (0.296 g, 0.0015 mol) in toluene (37.5 mL), these two solutions were attached to individual syringe pumps and added to vigorously stirring toluene in the 3-neck round-bottom flask at a rate of ~1 drop per 10 seconds simultaneously. After the addition of the reagents, the solution was allowed to stir for a 24 h period at room temperature. Silica gel (~0.50 g) was added to the solution and concentrated in vacuo and immediately subjected to column chromatography (EtOAc; $R_f = 0.12$). The product was isolated in 38% yield (0.2053 g) as a white solid. MP = 194-195 °C. ^{1}H NMR (500 MHz, chloroform-*d*) δ 4.25 (d, *J* = 13.9 Hz, 1H), 3.80 – 3.60 (m, 1H), 3.27 – 3.11 (m, 1H), 3.11 – 2.94 (m, 2H), 2.77 (d, *J* = 15.6 Hz, 1H), 2.74 – 2.64 (m, 1H), 2.64 – 2.53 (m, 1H), 2.52 – 2.26 (m, 2H), 2.26 – 2.05 (m, 2H), 2.04 – 1.72 (m, 2H), 1.71 – 1.47 (m, 1H), 1.47 – 1.20 (m, 1H). ^{13}C NMR (126 MHz, chloroform-*d*) δ 175.09, 52.43,

50.49, 33.48, 32.30, 31.34, 28.71, 28.44, 25.12. IR ν_{max} 2917, 2800, 1655, 1619, 1451, 1288, 1110, 919, 721 cm^{-1}. HRMS (EI+) *m/z* [M+1] calcd for $C_{17}H_{34}N_2S_2$ 359.1827, found 359.1816.

12,18-dithia-1,9-diazabicyclo[7.6.6]henicosane (L2). A 50 mL flame-dried round-bottom flask equipped with a magnetic stir bar, condenser, and nitrogen inlet was charged with 12,18-dithia-1,9-diazabicyclo[7.6.6]henicosane-2,8-dione (0.200 g, 0.466 mmol), dry toluene (27.0 mL), and borane dimethylsulfide (0.230 mL, 2.41 mmol). This solution was allowed to reflux for 2 h then cool to room temperature followed by the addition of triethanol amine (1.07 mL, 8.05 mmol). The solution was refluxed for an additional 4 h, after which the reaction was concentrated in vacuo and subjected to column chromatography (1:1; hexane:ethyl acetate, R_f = 0.35) to afford a white solid (0.1454 g) in 82% yield. MP = 76 – 78 °C. ^{1}H NMR (500 MHz, chloroform-*d*) δ 3.32 (ddd, *J* = 12.1, 10.2, 4.3 Hz, 1H), 2.99 (ddd, *J* = 11.4, 10.4, 5.6 Hz, 1H), 2.68 (ddd, *J* = 13.4, 8.7, 2.5 Hz, 1H), 2.59 (ddd, *J* = 7.4, 5.1, 2.2 Hz, 1H), 2.57 – 2.53 (m, 1H), 2.49 (ddd, *J* = 14.9, 6.0, 2.5 Hz, 1H), 2.41 (ddd, *J* = 12.8, 9.9, 2.7 Hz, 1H), 2.23 (dt, *J* = 7.2, 3.6 Hz, 1H), 2.21 – 2.16 (m, 2H), 1.83 – 1.72 (m, 1H), 1.57 (ddtd, *J* = 19.4, 8.5, 5.7, 2.7 Hz, 1H), 1.52 – 1.39 (m, 5H). ^{13}C NMR (126 MHz, chloroform-*d*) δ 59.66, 54.64, 54.55, 32.80, 30.50, 27.52, 27.45, 27.19, 26.89. IR ν_{max} 2929, 2854, 2790, 1652, 1548, 1448, 1369, 1282, 1014, 871 cm^{-1}. HRMS (EI+) *m/z* [M+1] calcd for $C_{17}H_{35}N_2S_4$ 331.2242, found 331.2240. **L2** (0.0327 g, 0.0989 mmol) was dissolved in methanol (1.00 mL) and added dropwise to a 10 mL round bottom flask that was charged with 1 M HCl in MeOH (5 mL) at 0 °C. The mixture was stirred for 5 min. and then concentrated in vacuo to afford 0.0399 g of **L2·HCl** (quantitative) as a white solid. ^{1}H NMR (500 MHz, deuterium oxide) δ 3.64 – 3.51 (m, 3H), 3.47 – 3.37 (m, 2H), 3.33 (dt, *J* = 14.2, 3.7 Hz, 1H), 3.29 – 3.13 (m, 3H), 2.91 – 2.82 (m, 1H), 2.23 (dq, *J* = 10.0, 5.5, 4.6 Hz, 2H), 2.00 – 1.85 (m, 1H), 1.71 – 1.55 (m, 2H), 1.48 (d, *J* = 7.2 Hz, 2H). ^{13}C NMR (126 MHz, d_2o) δ 56.81, 55.36, 53.91, 29.37, 28.41, 25.35, 25.28, 23.27, 21.09. HRMS (EI+) *m/z* [M+1] calcd for $C_{17}H_{35}N_2S_4$ 331.2242, found 331.2240.

14,20-dithia-1,11-diazabicyclo[9.6.6]tricosane-2,10-dione (L3). A 300 mL flame-dried 3-neck round-bottom flask equipped with a magnetic stir bar, nitrogen inlet, and three septa was charged with dry toluene (75 mL). A gas-tight syringe charged with 1,8-dithia-4,11-diazacyclotetradecane (0.352 g, 0.0015 mol), triethylamine (0.44 mL, 0.0030 mol) in toluene (37.5 mL) and a second gas-tight syringe was charged with azeloyl chloride (0.338 g, 0.0015 mol) in toluene (37.5 mL), these two solutions were attached to individual syringe pumps and added to vigorously stirring toluene in the 3-neck round-bottom flask at a rate of ~1 drop per 10 seconds simultaneously. After the addition of the reagents, the solution was allowed to stir for a 12 h period at room temperature. Silica gel (~2 g) was added to the solution and was concentrated in vacuo and immediately subjected to column chromatography (EtOAc; R_f = 0.49). The product was isolated in 62.5 % yield (0.3627 g) as a white solid. ^{1}H NMR (500 MHz, chloroform-*d*) δ 4.31 (t, *J* = 12.4 Hz, 1H), 4.18 (d, *J* = 13.7 Hz, 2H), 4.13 – 3.98 (m, 7H), 3.94 (d, *J* = 13.6 Hz, 4H), 3.74 (dq, *J* = 14.2, 8.7, 6.5 Hz, 8H), 3.34 (dd, *J* = 13.9, 5.9 Hz, 1H), 3.21 (ddd, *J* = 14.9, 11.7, 3.1 Hz, 3H), 3.15 – 2.85 (m, 16H), 2.85 – 2.74 (m, 13H), 2.74 – 2.39 (m, 32H), 2.39 – 2.29 (m, 3H), 2.24 (dt, *J* = 16.2, 5.9 Hz, 6H), 2.12 (dq, *J* = 15.9, 6.3, 5.4 Hz, 7H), 2.02 (dd, *J* = 18.5, 9.8 Hz, 4H), 1.99 – 1.89 (m, 9H), 1.83 (ddt, *J* = 14.6, 9.5, 4.8 Hz, 8H), 1.61 – 1.45 (m, 17H), 1.36 (ddd, *J* = 23.5, 16.1, 7.6 Hz, 14H), 1.13 (q, *J* = 11.2 Hz, 4H). ^{13}C NMR (126 MHz, chloroform-*d*) δ 174.82, 174.78, 174.55, 173.60, 52.09, 49.66, 48.97, 48.00, 46.14, 44.98, 43.56, 33.48, 32.85, 32.06, 31.79, 31.59, 31.40, 31.11, 30.78, 30.03, 29.68, 28.64, 28.38, 28.22, 28.03, 27.77, 27.57, 26.78, 26.69, 25.91, 24.77, 23.62,

22.58. IR ν_{max} 2923, 1639, 1417, 1367, 1272, 759 cm^{-1}. HRMS (EI+) *m/z* [M+] calcd for $C_{19}H_{34}N_2O_2S_2$ 386.2062, found 382.2056.

4, 20-dithia-1,11-diazabicyclo[9.6.6]tricosane (L4). A 50 mL flame-dried round-bottom flask equipped with a magnetic stir bar, condenser, and nitrogen inlet was charged with 14,20-dithia-1,11-diazabicyclo[9.6.6]tricosane-2,10-dione (0.180 g, 0.466 mmol), dry toluene (23.0 mL), and borane dimethylsulfide (0.200 mL, 2.12 mmol). This solution was allowed to reflux for 2 h then cool to room temperature followed by the addition of triethanol amine (0.63 mL, 4.72 mmol). The solution was refluxed for an additional 4 h, after which the reaction was concentrated in vacuo and subjected to column chromatography (1:1; hexane:ethyl acetate, R_f = 0.35) to afford a clear oil (0.112 g) in a 68% yield. IR ν_{max} 2915, 2850, 2792, 2345, 1454, 1376, 1292, 1095, 732 cm^{-1}. HRMS (EI+) *m/z* [M+1] calcd for $C_{19}H_{38}N_2S_2$ 359.2555, found 359.2553. **L4** (0.0355 g, 0.0989 mmol) was dissolved in methanol (1.00 mL) and added dropwise to a 10 mL round bottom flask that was charged with 1 M HCl in MeOH (5 mL) at 0 °C. The mixture was stirred for 5 min. and then concentrated in vacuo to afford 0.0427 g of **L4·HCl** (quantitative) as a white solid. ^{1}H NMR (500 MHz, deuterium oxide) δ 3.67 – 3.56 (m, 2H), 3.56 – 3.46 (m, 2H), 3.43 – 3.35 (m, 1H), 3.35 – 3.15 (m, 4H), 2.95 (ddd, *J* = 12.8, 8.3, 3.1 Hz, 1H), 2.22 (qq, *J* = 11.1, 6.3, 5.2 Hz, 2H), 1.85 – 1.70 (m, 2H), 1.44 (s, 1H), 1.38 (dd, *J* = 14.2, 6.5 Hz, 4H). ^{13}C NMR (126 MHz, deuterium oxide) δ 59.15, 55.61, 54.20, 31.89, 28.75, 26.65, 26.59, 25.54, 24.64, 22.48. HRMS (EI+) *m/z* [M+1] calcd for $C_{19}H_{38}N_2S_2$ 359.2555, found 359.2553.

General procedure for heavy metal chelation. A 10 mL pressure vessel equipped with a magnetic stir bar was charged with DMSO-*d6* (1.0 mL), lactam or cryptate (60 mM), and heavy metal (60 mM). This solution was warmed to 65 °C in an external oil bath for 5 min, cooled to room temperature and immediately transferred to an NMR tube.

L1·AgOTf. ^{1}H NMR (400 MHz, DMSO-*d6*) δ 11.96 (s, 1H), 4.21 (t, *J* = 13.0 Hz, 2H), 4.15 – 4.08 (m, 1H), 4.01 (ddd, *J* = 14.0, 4.1, 2.1 Hz, 9H), 3.89 (dd, *J* = 16.1, 8.2 Hz, 2H), 3.67 (dd, *J* = 14.9, 11.1 Hz, 11H), 3.27 – 3.18 (m, 1H), 3.09 (ddd, *J* = 15.0, 10.9, 2.2 Hz, 10H), 3.00 (dt, *J* = 15.2, 3.9 Hz, 10H), 2.91 – 2.84 (m, 5H), 2.83 – 2.73 (m, 11H), 2.72 – 2.64 (m, 12H), 2.48 (p, *J* = 1.8 Hz, 8H), 2.42 (td, *J* = 9.5, 4.7 Hz, 4H). ^{13}C NMR (101 MHz, DMSO-*d6*) δ 174.92, 51.65, 49.83, 33.87, 32.36, 32.10, 28.90, 28.51, 25.21. IR ν_{max} 2944, 2877, 2365, 1733, 1699, 1539, 1457, 1274, 1154, 983, 638 cm^{-1}. **Monomer**: HRMS (ESI) *m/z* [L+Ag]+ calcd for $C_{17}H_{30}N_2O_2S_2Ag$ 465.0794, found 465.0794. **Dimer**: HRMS (ESI) *m/z* [2L+Ag]+ calcd for $C_{34}H_{60}N_4O_4S_4Ag$ 823.2543, found 823.2547.

L1·Hg(NO$_3$)$_2$. ^{1}H NMR (400 MHz, DMSO-*d6*) δ 4.19 (t, *J* = 12.8 Hz, 2H), 4.05 (d, *J* = 12.2 Hz, 1H), 3.92 (dd, *J* = 16.2, 8.0 Hz, 1H), 3.67 (ddd, *J* = 14.5, 10.6, 2.9 Hz, 2H), 3.20 – 3.09 (m, 1H), 3.08 – 3.00 (m, 1H), 2.97 – 2.51 (m, 5H), 2.43 (dt, *J* = 9.7, 5.1 Hz, 1H), 2.27 – 1.90 (m, 4H), 1.79 (s, 2H), 1.65 (q, *J* = 7.5 Hz, 1H), 1.51 (t, *J* = 7.2 Hz, 0H), 1.40 (dt, *J* = 13.8, 6.7 Hz, 2H), 1.21 (p, *J* = 7.6 Hz, 2H). ^{13}C NMR (101 MHz, DMSO-*d6*) δ 175.01, 51.07, 49.63, 34.46, 34.05, 33.25, 32.43, 32.17, 29.98, 29.25, 28.63, 25.73, 25.24, 24.24. IR ν_{max} 2981, 2900, 2359, 1684, 1506, 1023, 817, 756, 639 cm^{-1}. HRMS (ESI) *m/z* [L+Hg+OH]+ calcd for $C_{17}H_{30}N_2O_3S_2Hg$ 577.1475, found 577.1477.

L1·Pb(NO$_3$)$_2$. ^{1}H NMR (400 MHz, DMSO-*d6*) δ 3.99 (ddd, *J* = 13.8, 4.3, 2.2 Hz, 2H), 3.95 – 3.85 (m, 0H), 3.66 (ddd, *J* = 14.6, 11.3, 2.7 Hz, 1H), 2.94 (ddd, *J* = 14.0, 11.0, 3.1 Hz, 2H), 2.84 (td, *J* = 9.9, 5.1 Hz, 1H), 2.79 – 2.50 (m, 3H), 2.42 (ddd, *J* = 14.5, 9.6, 5.1 Hz, 1H), 2.20 – 2.05 (m, 1H), 1.98 (dt, *J* = 14.6, 5.5 Hz, 1H), 1.73 – 1.58 (m, 1H), 1.36 (dq, *J* = 12.5, 7.1, 6.1 Hz, 1H), 1.19 (p, *J* = 8.1 Hz, 1H). ^{13}C NMR (101 MHz, DMSO-*d6*) δ 174.68, 52.30, 50.13, 33.26, 32.14, 31.08, 28.78, 28.64, 25.35. IR ν_{max} 2900, 2335, 1699, 1635, 1506, 1352, 1019, 976, 786 cm^{-1}. HRMS (ESI) *m/z* [L+Pb+NO$_3$]+ calcd for $C_{17}H_{30}N_3O_5S_2Pb$ 628.1387, found 628.1389.

L2·AgOTf. ^{1}H NMR (400 MHz, DMSO-*d6*) δ 3.47 (td, *J* = 10.5, 3.6 Hz, 1H), 3.02 (td, *J* = 10.3, 5.9 Hz, 1H), 2.92 – 2.62 (m, 3H), 2.57 – 2.49 (m, 1H), 2.46 – 2.37 (m, 1H), 2.32 – 2.21 (m, 1H), 2.14 (dd, *J* = 29.1, 12.9 Hz, 2H), 1.82 – 1.54 (m, 1H), 1.37 (s, 4H), 1.31 – 1.12 (m, 2H). ^{13}C NMR (101 MHz, DMSO-*d6*) δ 58.44, 54.03, 53.74, 33.88, 32.25, 27.58, 27.29, 27.26, 26.63. IR ν_{max} 2999, 2322, 1695, 1654, 1559, 1507, 1270, 988, 673 cm^{-1}. HRMS (ESI) *m/z* [L+Ag]+ calcd for $C_{17}H_{34}N_2S_2Ag$ 439.1203, found 439.1202.

L2·Hg(NO$_3$)$_2$. ^{1}H NMR (400 MHz, DMSO-*d6*) δ 8.37 (dd, *J* = 19.7, 10.9 Hz, 2H), 7.69 (s, 3H), 3.49 – 3.39 (m, 2H), 3.25 (d, *J* = 9.2 Hz, 1H), 3.07 – 2.86 (m, 7H), 2.76 – 2.64 (m, 1H), 2.45 – 2.39 (m, 1H), 2.20 (tt, *J* = 17.1, 9.0 Hz, 5H), 2.04 – 1.91 (m, 4H), 1.82 – 1.67 (m, 4H), 1.45 (s, 5H). ^{13}C NMR (101 MHz, DMSO-*d6*) δ 79.64, 54.89, 54.19, 54.04, 53.34, 52.42, 27.55, 26.04, 24.73. IR ν_{max} 2365, 2358, 2338, 1653, 1558, 1352, 1051, 1023, 982, 842, 818, 673, 654, 606 cm^{-1}. HRMS (ESI) *m/z* [L+Hg-C$_3$H$_5$]+ calcd for $C_{14}H_{29}N_2S_2Hg$ 491.1471, found 491.1475.

L2·Pb(NO$_3$)$_2$. ^{1}H NMR (400 MHz, DMSO-*d6*) δ 3.18 (ddd, *J* = 12.2, 10.2, 4.3 Hz, 1H), 2.96 (ddd, *J* = 11.8, 10.2, 5.6 Hz, 1H), 2.62 – 2.49 (m, 2H), 2.49 – 2.41 (m, 3H), 2.31 (ddd, *J* = 12.4, 9.3, 2.8 Hz, 1H), 2.19 (dd, *J* = 6.2, 3.0 Hz, 0H), 2.16 – 2.06 (m, 2H), 1.68 – 1.53 (m, 1H), 1.51 – 1.30 (m, 4H), 1.26 (p, *J* = 6.1, 5.6 Hz, 1H). ^{13}C NMR (101 MHz, DMSO-*d6*) δ 59.89, 54.53, 54.32, 32.59, 30.09, 27.52, 27.46, 27.22, 26.85. IR ν_{max} 2309, 1699, 1684, 1558, 1350, 1057, 980, 816, 617, 597 cm^{-1}. HRMS (ESI) *m/z* [L+Pb+NO$_4$]+ calcd for $C_{17}H_{34}N_3S_2O_4Pb$ 616.1751, found 616.1755.

L3·AgOTf. ^{1}H NMR (400 MHz, DMSO-*d6*) δ 4.13 – 3.99 (m, 4H), 3.98 – 3.91 (m, 2H), 3.75 (dd, *J* = 14.9, 7.6 Hz, 6H), 3.64 (s, 1H), 3.41 (dd, *J* = 15.6, 7.3 Hz, 2H), 3.08 (dt, *J* = 13.7, 6.1 Hz, 5H), 3.02 – 2.94 (m, 6H), 2.94 – 2.86 (m, 4H), 2.81 (d, *J* = 9.0 Hz, 7H), 2.74 – 2.67 (m, 1H), 2.66 – 2.57 (m, 5H), 2.32 – 2.18 (m, 2H), 2.19 – 2.03 (m, 4H), 2.00 – 1.83 (m, 3H), 1.83 – 1.52 (m, 2H), 1.47 – 1.05 (m, 10H). ^{13}C NMR (101 MHz, DMSO-*d6*) δ 174.34, 173.93, 173.80, 125.92, 122.72, 119.52, 116.31, 51.88, 49.52, 48.77, 48.53, 47.61, 46.44, 46.17, 33.94, 33.19, 32.95, 32.45, 31.95, 31.55, 30.64, 29.88, 29.57, 29.28, 28.53, 28.21, 27.89, 27.07, 26.69, 26.19, 24.56, 23.89, 22.99. IR ν_{max} 2811, 1633, 1275, 1220, 1153, 985 cm^{-1}. **Monomer**: HRMS (ESI) *m/z* [L+Ag]+ calcd for $C_{19}H_{34}N_2O_2S_2Ag$ 493.1107, found 493.1107. **Dimer**: HRMS (ESI) *m/z* [2L+Ag]+ calcd for $C_{38}H_{68}N_4O_4S_4Ag$ 881.3165, found 881.3171.

L3·Hg(NO$_3$)$_2$. ^{1}H NMR (400 MHz, DMSO-*d6*) δ 8.70 (s, 1H), 4.90 (t, *J* = 9.8 Hz, 2H), 4.55 (t, *J* = 5.4 Hz, 1H), 4.28 – 4.19 (m, 1H), 4.11 (t, *J* = 10.0 Hz, 1H), 3.96 – 3.53 (m, 4H), 3.42 – 3.19 (m, 3H), 3.07 – 2.99 (m, 2H), 2.98 – 2.54 (m, 9H), 2.32 (ddd, *J* = 10.5, 8.2, 4.9 Hz, 2H), 2.20 – 2.03 (m, 1H), 2.02 – 1.80 (m, 2H), 1.78 – 1.48 (m, 4H), 1.45 – 1.11 (m, 11H). ^{13}C NMR (101 MHz, DMSO-*d6*) δ 178.07, 175.46, 173.99, 173.45, 173.27, 173.10, 173.05, 172.86, 172.83, 79.62,

72.02, 69.74, 61.54, 60.23, 59.71, 53.07, 52.07, 48.71, 46.77, 46.58, 46.46, 46.03, 45.87, 45.77, 45.36, 44.84, 33.86, 33.78, 33.62, 33.58, 32.74, 31.91, 31.77, 31.49, 31.25, 30.21, 28.94, 28.88, 28.47, 28.42, 28.28, 28.24, 28.10, 28.07, 28.05, 27.84, 27.76, 27.58, 27.32, 26.75, 26.38, 26.28, 25.09, 24.60, 24.55, 24.40, 24.38, 24.23, 22.88, 19.48. IR ν_{max} 2987, 1737, 1636, 1355, 1017, 993 cm^{-1}. HRMS (ESI) *m/z* [L(D_3)+Hg+NO_3]+ calcd for $C_{19}H_{31}D_3N_3S_2O_5Hg$ 653.1828, found 653.1825.

L3·Pb(NO_3)$_2$. ^{1}H NMR (400 MHz, DMSO-*d6*) δ 4.04 – 3.97 (m, 1H), 3.93 – 3.74 (m, 4H), 3.66 (dt, *J* = 14.7, 7.1 Hz, 1H), 3.49 (dt, *J* = 15.0, 7.4 Hz, 1H), 3.01 (dt, *J* = 14.1, 7.0 Hz, 2H), 2.94 – 2.74 (m, 3H), 2.75 – 2.60 (m, 3H), 2.60 – 2.50 (m, 1H), 2.26 – 2.10 (m, 2H), 2.08 – 1.94 (m, 1H), 1.86 – 1.58 (m, 4H), 1.38 (s, 5H), 1.30 – 1.06 (m, 8H). ^{13}C NMR (101 MHz, DMSO-*d6*) δ 173.88, 173.31, 52.12, 49.61, 48.80, 46.38, 45.86, 45.14, 32.46, 31.73, 31.48, 31.40, 31.20, 31.11, 30.13, 28.86, 27.39, 26.76, 26.44, 25.23, 22.87. IR ν_{max} 2901, 1730, 1516, 1155, 1003, 779 cm^{-1}. **Monomer**: HRMS (ESI) *m/z* [L+Pb+NO_3]+ calcd for $C_{19}H_{34}N_3O_5S_2Pb$ 656.1701, found 656.1694. **Dimer**: HRMS (ESI) *m/z* [2L+Pb+NO_3]+ calcd for $C_{38}H_{68}N_5O_7S_4Pb$ 1042.3763, found 1042.3756.

L4·AgOTf. ^{1}H NMR (400 MHz, DMSO-*d6*) δ 3.29 – 3.07 (m, 1H), 2.92 (s, 4H), 2.82 (s, 1H), 2.76 – 2.65 (m, 1H), 2.56 (s, 3H), 2.45 – 2.30 (m, 3H), 2.27 – 2.19 (m, 2H), 1.99 – 1.69 (m, 4H), 1.59 – 1.24 (m, 19H). ^{13}C NMR (101 MHz, DMSO-*d6*) δ 125.93, 122.73, 119.52, 116.32, 53.61, 33.59, 32.06, 27.60, 27.31, 26.84, 26.64, 25.88. IR ν_{max} 2956, 2366, 2359, 1653, 1456, 1274, 1224, 981, 638 cm^{-1}. HRMS (ESI) *m/z* [L+Ag]+ calcd for $C_{19}H_{38}N_2S_2Ag$ 467.1517, found 467.1516.

L4·Hg(NO_3)$_2$. ^{1}H NMR (400 MHz, DMSO-*d6*) δ 7.43 (s, 4H), 3.58 – 3.36 (m, 1H), 3.21 – 3.08 (m, 7H), 3.08 – 2.99 (m, 4H), 2.98 – 2.85 (m, 1H), 2.85 – 2.69 (m, 2H), 2.63 (dt, *J* = 11.5, 4.4 Hz, 10H), 2.42 – 2.13 (m, 7H), 2.12 – 1.82 (m, 7H), 1.81 – 1.73 (m, 2H), 1.52 – 1.14 (m, 10H). ^{13}C NMR (101 MHz, DMSO-*d6*) δ 57.80, 55.92, 54.78, 54.08, 52.37, 52.12, 51.74, 35.64, 32.92, 29.72, 27.88, 26.95, 25.87. IR ν_{max} 2993, 2356, 2350, 1716, 1682, 1355, 1061, 1032, 957 cm^{-1}. HRMS (ESI) *m/z* [L+Hg-C_3H_5]+ calcd for $C_{16}H_{33}N_2S_2Hg$ 519.1784, found 519.1785.

Computational Details

An exhaustive mapping of conformational space was performed by decomposing the parent cryptand into three independent chains. A torsion scan was performed on each chain and these chains are then put together combinatorially. The resulting molecules were then optimized at the B97-D/def2-TZVP level of theory,[34] accounting for solvent effects with IEF-PCM[35] (using chloroform as solvent). Geometries, vibrational frequencies, and thermal free energy corrections (298K) were computed at the same level of theory. Representative transition state (TS) structures connecting selected energy minima were verified by the presence of a single imaginary vibrational frequency. Thermal free energy corrections were based on the quasi-rigid rotor/harmonic oscillator (quasi-RRHO) approximation of Grimme.[36] The final presented free energies were computed at the PCM-ωB97X-D/def2-TZVP//PCM-B97-D/def2-TZVP level of theory.[37] Gas phase binding energies were computed at ωB97X-D/def2-TZVP//PCM-B97-D/def2-TZVP level of theory.[38] All the computations were performed using Gaussian 09[39] and the B97-D computations employed density fitting techniques. Molecular structure figures were generated using CYLview.

Acknowledgements

We thank Indiana University Mass Spectrometry Facility in Bloomington, IN for exact mass measurements. This study was also supported in part by resources and technical expertise from the Georgia Advanced Computing Resource Center, a partnership between the University of Georgia's Office of the Vice President for Research and Office of the Vice President for Information Technology. We would also like to acknowledge the National Science Foundation (CHE-0840446) for funds used to purchase the Bruker APEX II Duo X-ray diffractometer used in this research.

Supplementary Data

^{1}H, ^{13}C, COSY, HSQC, and HMBC including VT spectrum, X-Ray crystallography, IR, HRMS, additional computational details; absolute free energies; and Cartesian coordinates. This material is available free of charge via the internet at

References and Notes

1 a) C. J. Pedersen, Cyclic polyethers and their complexes with metal salts, *J. Am. Chem. Soc.,* 1967, **89**, 2495-2496. b) C. J. Pedersen, Cyclic polyethers and their complexes with metal salts, *J. Am. Chem. Soc.* 1967, **89**, 7017-7036.

2 B. Dietrich, J. M. Lehn, and J. P. Sauvage, Diaza-polyoxa-macrocycles et macrobicycles *Tetrahedron Lett.,* 1969, **10**, 2885-2888 and 2889-2892.

3 D. J. Cram, T. Kaneda, R. C. Helgeson, and G. M. Lein, Spherands - ligands whose binding of cations relieves enforced electron-electron repulsions, *J. Am. Chem. Soc.,* 1979**, 101***,* 6752-6754.

4 R. M. MacDonald, M. E. Fieser, J. E. Bates,.; Ziller, and F. Furche, Completing the Series of +2 Ions for the Lanthanide Elements: Synthesis of Molecular Complexes of Pr^{2+}, Gd^{2+}, Tb^{2+}, and Lu^{2+}, *J. Am. Chem. Soc.,* 2013, **135**, 13310-13313.

5 J. M. Lehn, Cryptates: macropolycyclic inclusion complexes, *Pure & Appl. Chem.,* 1977, **49**, 857-870.

6 a) D. J. Cram, and J. M. Cram, Host-Guest Chemistry: Complexes between organic compounds simulate the substrate selectivity of enzymes, *Science,* 1974**, 183***,* 803-809. b) E. P. Kyba, R. C. Helgeson, K. Madan, G. W. Gokel, T. L. Tarnowski, S. S. Moore, and D. J. Cram, Host-guest complexation. 1. Concept and illustration, *J. Am. Chem. Soc.,* 1977**, 99***,* 2564-2571. c) Topics in Current Chemistry, "Host-Guest Complex", Volumes I-III, ed. E. L. Boschke, Springer Verlag, Berlin, 1982-1984.

7 a) G. Alibrandi, V. Amendola, G. Bergamaschi, L. Fabbrizzi, and M. Licchelli, Bistren cryptands and cryptates: versatile receptors for anion inclusion and recognition in water, *Org. Biomol. Chem.,* 2015, **13**, 3510-3524. b) J. L. Dye, C. W. Andrews, and S. E. Mathews, Strategies for the

preparation of compounds of alkali metal anions, *J. Phys. Chem.*, 1975, **79**, 3065-3070. c) P. Paul, and K. Nag, Sulfur-nitrogen-bonded metal chelates. 16. Reactivities of coordinated nitriles in the nickel(II) complexes [Ni(SNN)(NCR)](ClO_4) with alcohols, amines, and different nucleophiles. Synthesis, characterization, and stereochemistry of imino-ether, amide, and amidine complexes, *Inorg. Chem.,* 1987, **26**, 1586-1592.

8 a) N. H. Evans, and P. D. Beer, Advances in Anion Supramolecular Chemistry: From Recognition to Chemical Applications, *Angewandte Chemie*, 2014, **53**, 11716-11754. b) N. Vasdev, P. P. Cao, E. M. Oosten, A. A. Wilson, S. Houle, G. Hao, X. Sun, N. Slavine, M. Alhasan, P. P. Antich, F. J. Bonte, and P. Kulkarni, Synthesis and PET imaging studies of [^{18}F]2-fluoroquinolin-8-ol ([^{18}F]CABS13) in transgenic mouse models of Alzheimer's disease, *Med. Chem. Commun.,* 2012, **3**, 1228-1230.

9 V. M. Cangelosi, T. G. Carter, J. L. Crossland, L. N. Zakharov, and D. W. Johnson, Self-Assembled E_2L_3 Cryptands (E = P, As, Sb, Bi): Transmetalation, Homo- and Heterometallic Assemblies, and Conformational Isomerism *Inorg. Chem.,* 2010, **49**, 9985-9992.

10 S. Bhattacharyya, and M. Dixit, Metallic radionuclides in the development of diagnostic and therapeutic radiopharmaceuticals, *Dalton Trans.,* 2011, **40**, 6112– 6128.

11 C. J. Anderson, and M. J. Welch, Radiometal-Labeled Agents (Non-Technetium) for Diagnostic Imaging, *Chem. Rev.,* 1999, **99**, 2219–2234.

12 R. Ferdani, D. J. Stigers, A. L. Fiamengo, L. Wei, B. T. Y. Li, J. A. Golen, A. L. Rheingold, G. R. Weisman, E. H. Wong, and C. J. Anderson, Synthesis, Cu(II) complexation, ^{64}Cu-labeling and biological evaluation of cross-bridged cyclam chelators with phosphonate pendant arms. *Dalton Trans*., 2012, **41**, 1938.

13 a) G. R. Walke, and S. Ruthstein, Does the ATSM-Cu(II) Biomarker Integrate into the Human Cellular Copper Cycle?, *ACS Omega,* 2019, **4**, 12278-12285. b) J. M. Floberg, L. Wang, N. Bandara, R. Rashimi, C. Mpoy, J. R. Garbow, B. E. Rogers, G. J. Patti, and J. K. Schwarz, Altering cellular reducing potential changes ^{64}Cu-ATSM signal with or without hypoxia, *J. Nucl. Med.,* 2019, doi: 10.2967/jnumed.119.230805. c) P. J. Blower, T. C. Castle, A. R. Cowley, J. R. Dilworth, P. S. Donnelly, E. Labisbal, F. E. Sowery, S. J. Teat, and M. J. Went, Structural trends in copper(II) bis(thiosemicarbazone) radiopharmaceuticals, *Dalton Trans.,* 2003, **23**, 4416-4425.

14 A. L. Vāvere, and J. S. Lewis, Cu-ATSM: a radiopharmaceutical for the PET imaging of hypoxia, *Dalton Trans.,* 2007, 4893-4902.

15 a) G. R. Weisman, M. E. Rogers, E. H. Wong, J. P. Jasinski, and E. S. Paight, Cross-Bridged Cyclam. Protonation and Li^+ Complexation in a Diamond-Lattice Cleft, *J. Am. Chem. Soc.,* 1990, **112(23)**, 8604-8605. b) E. H. Wong, G. R. Weisman, D. C. Hill, D. P. Reed, M. E. Rogers, J. S. Condon, M. A. Fagan, J. C. Calabrese, K-C. Lam, I. A. Guzei, and A. L. Rheingold, Synthesis and characterization of cross-bridged cyclams and pendant-armed derivatives and structural studies of their copper (II) complexes, *J. Am. Chem. Soc.,* 2000, **122**, 10561-10572.

16 C. J. Anderson, T. J. Wadas, E. H. Wong, and G. R. Weisman, Cross-bridged Macrocyclic Chelators for Stable Complexation of Copper Radionuclides for PET Imaging, *Nucl Med Mol Imaging,* 2008, **52**, 185-192.

17 J. E. Sprague, Y. Peng, X. Sun, G. R. Weisman, E. H. Wong, S. Achilefu, and C. J. Anderson, Preparation and Biological Evaluation of Copper-64–Labeled Tyr^3-Octreotate Using a Cross-Bridged Macrocyclic Chelator, *Clinical Cancer Research,* 2004, **10**, 8674-8682.

18 C. Foerster, J. C. Knight, M. Wuest, B. Rowan, S. E. Lapi, A. J. Amoroso, P. G. Edwards, and F. Wuest, Synthesis, complex stability and small animal PET imaging of a novel ^{64}Cu-labelled cryptand molecule, *Med. Chem. Commun.*, 2014, **5**, 958-962.

19 a) S. O. Kang, J. M. Llinares, D. Powell, D. VanderVelde, and K. Bowman-James, New Polyamide Cryptand for Anion Binding, *J. Am. Chem. Soc.,* 2003, **125**, 10152-10153. b) B. Sarkar, P. Mukhopadhyay, P. K. Bharadwaj, Laterally non-symmetric aza-cryptands: synthesis, catalysis and derivatization to new receptors, *Coordin. Chem. Rev.,* 2003, **236**, 1-13.

20 P. Auffinger, and G. Wipff, Molecular dynamics simulations on the protonated 222. H^+ and 222.2H^+ cryptands in water: Endo versus exo conformations, *J. Incl. Phenom. Mol. Recognit. Chem.,* 1991, **11**, 71-88.

21 R. W. Alder, and S. P. East, *In/Out* Isomerism *Chem. Rev.,* 1996, **96***,* 2097-2111.

22 G. Meurant, *Stereochemical and Stereophysical Behavior of Macrocycles* Elsevier, Amsterdam, Netherlands, 2012, 15-85.

23 R. C. Reid, M-K. Yau, R. Sing, J. Lim, and D. P. Fairlie, Potent Heterocyclic Ligands for Human Complement C3a Receptor, *J. Am. Chem. Soc.,* 2014, **136**, 11914-11917.

24 a) K. Krakowiak, J. Bradshaw, A. Haoyun, and R. Izatt, Simple Methods for the preparation of cryptands, *Pure & Appl. Chem.,* 1993, **65**, 511-514. b) F. Huang, H. Gibson, W. S. Bryant, D. S. Nagvekar, and F. R. Fronczek, First pseudorotaxane-like [3]complexes based on cryptands and paraquat: self-assembly and crystal structures, *J. Am. Chem. Soc.,* 2003, **123**, 9367-9371.

25 T. L. Walker, W. Malasi, S. Bhide, T. Parker, D. Zhang, A. Freedman, J. M. Modarelli, J. T. Engle, C. J. Ziegler, P. Custer, W. J. Youngs, and M. J. Taschner, Synthesis and characterization of 1,8-dithia-4,11-diazacyclotetradecane, *Tet. Lett.,* 2012, **53**, 6548-6551.

26 B. Dietrich, P. Viout, and J. M. Lehn, *Macrocyclic Chemistry*; VCH, Weinheim, Germany, 1993, 384.

27 B. G. Cox, J. Murray-Rust, P. Murray-Rust, N. Truong, and H. Schneider, Kinetics and mechanisms of formation of the di-endo protonated cryptand (2,1,1)H_2^{2+} including trapping and X-ray structure determination as its diperchlorate salt, *Chem. Soc., Chem. Comm.,* 1982, **7**, 377-379.

28 T. L. Walker, I. S. Taschner, S. M. Chandra, M. J. Taschner, J. T. Engle, B. R. Schrage, C. J. Ziegler, X. Gao, and S. E. Wheeler, Lone-Pair-Induced Topicity Observed in Macrobicyclic Tetrathia Lactams and Cryptands: Synthesis, Spectral Identification, and Computational Assessment, *J. Org. Chem.,* 2018, **83**, 10025-10036.

29 a) R. E. Wolf Jr., J. R. Hartman, J. M. E. Storey, B. M. Foxman, and S. R. Cooper, Crown thioether chemistry: structural and conformational studies of tetrathia-12-crown-4, pentathia-15-crown-5, and hexathia-18-crown-6. Implications for ligand design, *J. Am. Chem. Soc.,* 1987, **109**(14), 4328-4335. b) S. E. Hill, and D. Feller, Theoretical Conformational Analysis of Thiacrown Macrocycles, *J. Phys. Chem. A*., 2000, **104**, 652-660.

30 S. Y. Lee, S. Park, and S. S. Lee, Copper(I), silver(I), and palladium(II) complexes of a thiaoxamacrocycle displaying unusual topologies, *Inorg. Chem.,* 2009, **48**(23), 11335-11341.

31 X. Wang, H. Wang, and Y. Tan, DFT study of the cryptand and benzocryptand and their complexes with alkali metal cations: Li^+, Na^+, K^+, *J. Comput. Chem.,* 2008, **29**, 1423-1428.

32 X. X. Zhang, R. M. Izatt, J. S. Bradshaw, and K. E. Krakowiak, Approaches to improvement of metal ion selectivity by cryptands, *Coord. Chem. Rev.,* 1998, **174**, 179-189.

33 S. O. Kang, J. M. Llinares, D. Powell, D. VanderVelde, and K. Bowman-James, New Polyamide Cryptand for anion binding, *J. Am. Chem. Soc.,* 2003, **125**, 10152-10153.

34 (a) A. Becke, Density-functional thermochemistry. V. Systematic optimization of exchange-correlation functionals, *J. Chem. Phys.,* 1997, **107**, 8554-8560. (b) S. Grimme, Semiempirical GGA-type density functional constructed with a long-range dispersion correction, *J. Comp. Chem.,* 2006, **27**, 1787-1799. (c) F. Weigend, and R. Ahlrichs, Balanced basis sets of split valence, triple zeta valence and quadruple zeta valence quality for H to Rn: Design and assessment of accuracy, *Phys. Chem. Chem. Phys.,* 2005, **7**, 3297-3305.

35 (a) S. Miertus, E. Scrocco, and J. Tomasi, Electrostatic interaction of a solute with a continuum. A direct utilizaion of AB initio molecular potentials for the prevision of solvent effects, *Chem. Phys.,* 1981, **55**, 117-129. (b) J. Tomasi, B. Mennucci, and R. Cammi, Quantum mechanical continuum solvation models, *Chem. Rev.,* 2005, **105**, 2999-3093.

36 S. Grimme, Supramolecular Binding Thermodynamics by Dispersion-Corrected Density Functional Theory, *Chem. Eur. J.,* 2012, **18**, 9955-9964.

37 J. -D. Chai, and M. Head-Gordon, Systematic optimization of long-range corrected hybrid density functionals, *J. Chem. Phys.,* 2008, **128**, 084106.

38 J. -D. Chai, and M. Head-Gordon, Systematic optimization of long-range corrected hybrid density functionals, *J. Chem. Phys.,* 2008, **128**, 084106.

39 M. J. Frisch, G. W. Trucks, H. B. Schlegel, G. E. Scuseria, M. A. Robb, J. R. Cheeseman, G. Scalmani, V. Barone, B. Mennucci, G. A. Petersson, H. Nakatsuji, M. Caricato, X. Li, H. P. Hratchian, A. F. Izmaylov, J. Bloino, G. Zheng, J. L. Sonnenberg, M. Hada, M. Ehara, K. Toyota,

R. Fukuda, J. Hasegawa, M. Ishida, T. Nakajima, Y. Honda, O. Kitao, H. Nakai, T. Vreven, J. A. Montgomery, J. E. Peralta, F. Ogliaro, M. Bearpark, J. J. Heyd, E. Brothers, K. N. Kudin, V. N. Staroverov, R. Kobayashi, J. Normand, K. Raghavachari, A. Rendell, J. C. Burant, S. S. Iyengar, J. Tomasi, M. Cossi, N. Rega, J. M. Millam, M. Klene, J. E. Knox, J. B. Cross, V. Bakken, C. Adamo, J. Jaramillo, R. Gomperts, R. E. Stratmann, O. Yazyev, A. J. Austin, R. Cammi, C. Pomelli, J. W. Ochterski, R. L. Martin, K. Morokuma, V. G. Zakrzewski, G. A. Voth, P. Salvador, J. J. Dannenberg, S. Dapprich, A. D. Daniels, J. B. Foresman, J. V. Ortiz, J. Cioslowski, and D. J. Fox, Gaussian 09, Revision B.01. Wallingford CT, 2009.